

Article

Investigation of Antifungal Properties of Synthetic Dimethyl-4-Bromo-1-(Substituted Benzoyl) Pyrrolo[1,2-a] Quinoline-2,3-Dicarboxylates Analogues: Molecular Docking Studies and Conceptual DFT-Based Chemical Reactivity Descriptors and Pharmacokinetics Evaluation

Vijayakumar Uppar ^{1,†}, Sandeep Chandrashekharappa ^{2,3,†}, Chandan Shivamallu ⁴, Sushma P ³, Shiva Prasad Kollur ⁵, Joaquín Ortega-Castro ⁶, Juan Frau ⁶, Norma Flores-Holguín ⁷, Atiyaparveen I. Basarikatti ¹, Mallikarjun Chougala ⁸, Mrudula Mohan M ⁴, Govindappa Banuprakash ⁹, Jayadev ⁹, Katharigatta N. Venugopala ^{10,15}, Belakatte P. Nandeshwarappa ¹¹, Ravindra Veerapur ¹², Abdulaziz A. Al-Kheraif ¹³, Abdallah M. Elgorban ¹⁴, Asad Syed ¹⁴, Kiran K. Mudnakudu-Nagaraju ^{4,*}, Basavaraj Padmashali ^{1,*} and Daniel Glossman-Mitnik ⁷



Citation: Uppar, V.; Chandrashekharappa, S.; Shivamallu, C.; P, S.; Kollur, S.P.; Ortega-Castro, J.; Frau, J.; Flores-Holguín, N.; Basarikatti, A.I.; Chougala, M.; et al. Investigation of Antifungal Properties of Synthetic Dimethyl-4-Bromo-1-(Substituted Benzoyl) Pyrrolo[1,2-a] Quinoline-2,3-Dicarboxylates Analogues: Molecular Docking Studies and Conceptual DFT-Based Chemical Reactivity Descriptors and Pharmacokinetics Evaluation. *Molecules* **2021**, *26*, 2722. <https://doi.org/10.3390/molecules26092722>

Academic Editor: Jan Brezovsky

Received: 18 January 2021

Accepted: 2 March 2021

Published: 6 May 2021

Publisher's Note: MDPI stays neutral with regard to jurisdictional claims in published maps and institutional affiliations.



Copyright: © 2021 by the authors. Licensee MDPI, Basel, Switzerland. This article is an open access article distributed under the terms and conditions of the Creative Commons Attribution (CC BY) license (<https://creativecommons.org/licenses/by/4.0/>).

- ¹ Department of Chemistry, School of Basic Science, Rani Channamma University, Belagavi 591156, Karnataka, India; vijay.uppar@gmail.com (V.U.); atiyabasarikatti59@gmail.com (A.I.B.)
- ² Institute for Stem Cell Science and Regenerative Medicine, NCBS, TIFR, GKVK-Campus Bellary road, Bengaluru 560065, Karnataka, India; sandeep_m7@rediffmail.com
- ³ Department of Medicinal Chemistry, National Institute of Pharmaceutical Education and Research (NIPER) Raebareli, Lucknow (UP) 226002, India; sushmap@jssuni.edu.in
- ⁴ Department of Biotechnology & Bioinformatics, Faculty of Life Sciences, JSS Academy of Higher Education and Research, Mysore 570015, Karnataka, India; chandans@jssuni.edu.in (C.S.); mrudula51219@gmail.com (M.M.M.)
- ⁵ Department of Sciences, Amrita School of Arts and Sciences, Amrita Vishwa Vidyapeetham, Mysuru 570026, Karnataka, India; shivachemist@gmail.com
- ⁶ Departament de Química, Universitat de les Illes Balears, E-07122 Palma de Mallorca, Spain; joaquin.castro@uib.es (J.O.-C.); juan.frau@uib.es (J.F.)
- ⁷ Laboratorio Virtual NANOCOSMOS, Departamento de Medio Ambiente y Energía, Centro de Investigación en Materiales Avanzados, Chihuahua, Chih 31136, Mexico; norma.flores@cimav.edu.mx (N.F.-H.); dglossman@gmail.com (D.G.-M.)
- ⁸ Department of Biotechnology, JSS College of Arts, Commerce and Science (Autonomous), Mysore 570025, Karnataka, India; mallikarjun100@gmail.com
- ⁹ Department of Chemistry, SJB Institute of Technology, Bengaluru 560060, Kengeri, India; gbanuprakash@sjbit.edu.in (G.B.); jayadev@sjbit.edu.in (J.)
- ¹⁰ Department of Pharmaceutical Sciences, College of Clinical Pharmacy, King Faisal University, Al-Ahsa 31982, Saudi Arabia; kvenugopala@kfu.edu.sa
- ¹¹ Department of Studies in Chemistry, Shivagangothri, Davangere University, Davangere 577007, Karnataka, India; belakatte@davangereuniversity.ac.in
- ¹² Department of Metallurgy and Materials Engineering, Malawi Institute of Technology, Malawi University of Science and Technology, P.O. Box-5916 Limbe, Malawi; rveerapur@must.ac.mw
- ¹³ Dental Biomaterials Research Chair, Dental Health Department, College of Applied Medical Sciences, King Saud University, P.O. Box 10219, Riyadh 11433, Saudi Arabia; aalkhuraif@ksu.edu.sa
- ¹⁴ Department of Botany and Microbiology, College of Science, King Saud University, P.O. Box 2455, Riyadh 11451, Saudi Arabia; aelgorban@ksu.edu.sa (A.M.E.); assyed@ksu.edu.sa (A.S.)
- ¹⁵ Department of Biotechnology and Food Technology, Faculty of Applied Sciences, Durban University of Technology, Durban 4001, South Africa
- * Correspondence: kirankumarmn@jssuni.edu.in (K.K.M.-N.); basavarajpadmashali@yahoo.com (B.P.)
- † These authors contributed equally to this work.

Abstract: *Candida albicans*, an opportunistic fungal pathogen, frequently colonizes immune-compromised patients and causes mild to severe systemic reactions. Only few antifungal drugs are currently in use for therapeutic treatment. However, evolution of a drug-resistant *C. albicans* fungal pathogen is of major concern in the treatment of patients, hence the clinical need for novel drug design and development. In this study, in vitro *screening* of novel putative pyrrolo[1,2-a]quinoline derivatives as the lead drug targets and in silico prediction of the binding potential of these lead molecules

against *C. albicans* pathogenic proteins, such as secreted aspartic protease 3 (SAP3; 2H6T), surface protein β -glucanase (3N9K) and sterol 14- α demethylase (5TZ1), were carried out by molecular docking analyses. Further, biological activity-based QSAR and theoretical pharmacokinetic analysis were analyzed. Here, in vitro screening of novel analogue derivatives as drug targets against *C. albicans* showed inhibitory potential in the concentration of 0.4 μ g for BQ-06, 07 and 08, 0.8 μ g for BQ-01, 03, and 05, 1.6 μ g for BQ-04 and 12.5 μ g for BQ-02 in comparison to the standard antifungal drug fluconazole in the concentration of 30 μ g. Further, in silico analysis of BQ-01, 03, 05 and 07 analogues docked on chimeric 2H6T, 3N9K and 5TZ1 revealed that these analogues show potential binding affinity, which is different from the therapeutic antifungal drug fluconazole. In addition, these molecules possess good drug-like properties based on the determination of conceptual Density Functional Theory (DFT)-based descriptors, QSAR and pharmacokinetics. Thus, the study offers significant insight into employing pyrrolo[1,2-*a*]quinoline analogues as novel antifungal agents against *C. albicans* that warrants further investigation.

Keywords: BQ molecules; pyrrolo[1,2-*a*] quinolone; indolizines; molecular docking; DFT—density functional theory; conceptual DFT; *Candida albicans*; antifungal drug

1. Introduction

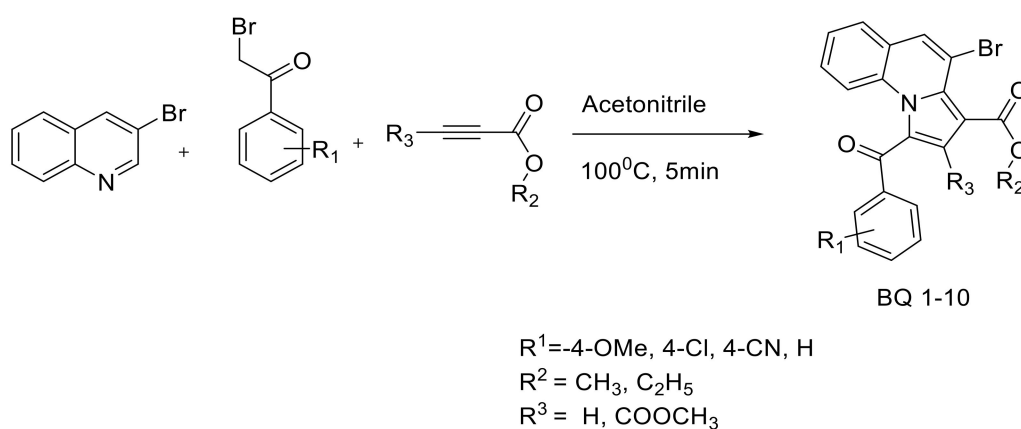
Globally, *Candida albicans* (*C. albicans*) is a genus of yeast that frequently causes nosocomial fungal infection in patients with a defined clinical condition—i.e., invasive candidiasis and candidemia [1,2]. Being an opportunistic fungal pathogen, *C. albicans* asymptotically colonized mucosal surfaces of the skin, vagina, mouth, and intestine in patients suffering from invasive candidiasis as well as systemically colonizes the bloodstream in candidemia patients and poses a major therapeutic challenge in medically and immune-compromised patients, with a mortality rate of 30–40% [3–6]. Further, *C. albicans* frequently infects humans with pre-existing conditions due to overuse of broad-spectrum antibiotics and immunosuppressants, surgical intervention, diabetes, prolonged hospitalization, and radio- as well as chemotherapy (in case of malignancy) [7,8]. Until now, reports suggested that only few classes of potential antifungal drugs such as azoles, echinocandins, and polyenes are on demand for the treatment of fungal infections and that multidrug resistance fungal pathogens are increasing worldwide along with adverse as well as cytotoxic effects [9–11].

The innate immune response predominates in regulating *C. albicans* fungal infectivity in normal individuals [12]. However, in the state of immune dysfunction, fungus invasion results due to switching of yeast to hyphal growth formations, which enter the human body via pathogen recognition factors present on various immune cells, which induces immune reactivity causing a wide range of symptoms from superficial to major life-threatening systemic reactions [3]. However, the number of antifungal drugs in treatment are very limited [13] and therefore, new therapies for fungal infection are of public concern as drug-resistant *C. albicans* are increasing worldwide [9,14,15].

However, in organic chemistry, the maximum heterocyclic compounds possess significant biological activity [16–36]. Recent reports suggest that indolizine is a very attractive molecule among the heterocyclic compounds and possesses two fused ring structures with carbon and nitrogen bridging atoms. Further, the numerous indolizine derivatives show potential biological activities [16,21–41], which includes antioxidant [42–44], antimicrobial [42–46], anti-inflammatory [47], anticancer [48,49] and antituberculosis [50] activities.

Pyrrolo[1,2-*a*]quinoline and pyrrolo[1,2-*a*]isoquinoline are family members of indolizine that are also known as 5,6-benzo-fused indolizine and 7,8-benzo-fused indolizine, respectively [51]. The series of these analogues has shown remarkable biological activity so far [52]. For instance, recent publications from V. Uppar et al. (2020) and others shows that pyrrolo[1,2-*a*]quinoline derivatives effectively inhibit the activity of microbial pathogens such as bacteria (both Gram-positive and Gram-negative) [44,53–56], and fungus [57],

followed by various disease conditions such as cancer [58], malaria [59], inflammation [60] and Alzheimer disease [61]. In addition, these derivatives possess antioxidant activity [44,54–56]. Further, ethyl-1-(subbenzoyl)-5-methylpyrrolo[1,2-a]quinoline-3-carboxylate and dimethyl 1-(subbenzoyl)-5-methylpyrrolo[1,2-a]quinoline-2,3-dicarboxylate derivatives have been tested for their larvicidal activity against *Anopheles arabiensis* [56]. Collectively, the broad-spectrum nature of the compounds intensified further to investigate whether newly synthesized derivatives target *C. albicans* fungal pathogens. Herein, the synthesized dimethyl-4-bromo-1-(4-substituted benzoyl) pyrrolo[1,2-a]quinoline-2,3-dicarboxylate methyl 4-bromo-1-(4-sub-benzoyl)pyrrolo[1,2-a]quinoline-3-carboxylate 1a-n (Scheme 1) [55], a novel analogue derivative (Figure 1), was tested for its inhibitory activity against *C. albicans* in vitro. As shown in Figure 1, these derivatives consist of methyl ester groups present at the second and third positions (highlighted) of BQ-01, 03, 05 and 07, and only one ester group at the third position of BQ-02, 04, 06 and 08.



Scheme 1. Synthetic scheme for the construction of dimethyl-4-bromo-1-(substituted benzoyl)pyrrolo[1,2-a]quinoline-2,3-dicarboxylate [44].

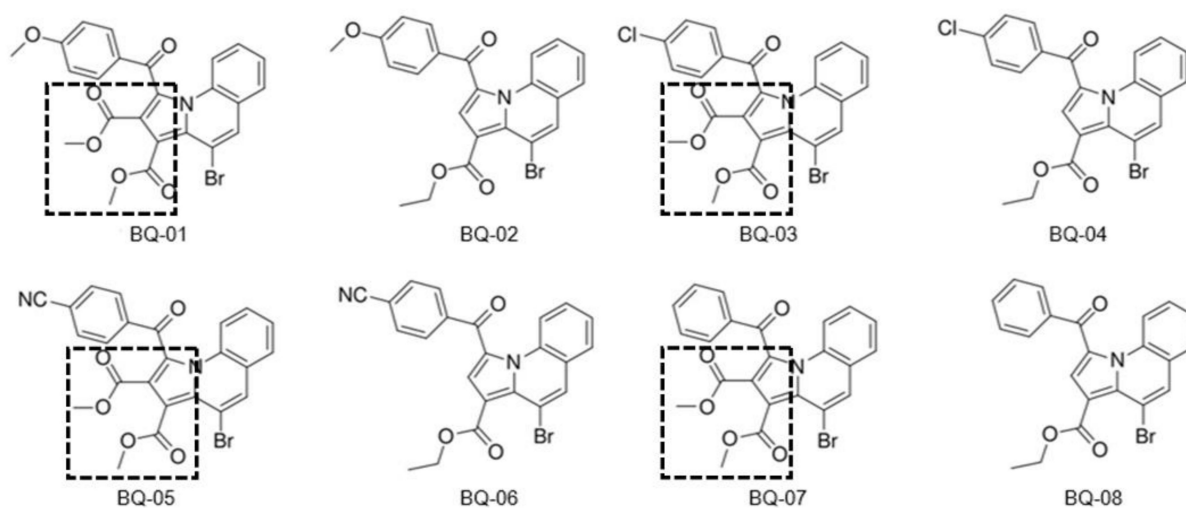


Figure 1. Molecular structures and codes of pyrrolo[1,2-a]quinoline derivatives used for their in vitro antifungal activity [44]. All the eight pyrrolo[1,2-a]quinoline derivatives possess common bromo substituents at the fourth position. The four compounds, namely, BQ-01, 03, 05 and 07, consist of methyl ester groups at the second and third positions; in comparison, BQ-02, 04, 06 and 08 possess hydrogen groups at the second position and ethyl esters at third position, respectively. Further, BQ-01, 03, 05 and 07 consist of two ester groups at second and third positions (as highlighted), which donate two electrons, and only one electron donor group present at the third positions of the BQ-02, 04, 06 and 08 derivatives.

Furthermore, chemoinformatic methods are utilized for the study and organization of chemical information, a tool widely used for the development of new medical drugs

in the pharmaceutical industry. Here, chemoinformatics are applied for the prediction of the molecular properties of many systems based on the knowledge of previously studied molecular structures and computational displaying of the same by considering the close relationship between biological data and organic structures and energies. The literature suggests that the molecular descriptors can be related to molecular properties [62].

In the present study, compounds tested in vitro were analyzed to elucidate their mechanisms of action by employing in silico molecular docking calculations. In addition, the present work reports the information on the chemical reactivity of the molecules under study through Density Functional Theory (DFT) derived concepts, which shows correlation of their biological activity [63–69]. Further, the chemical reactivity properties of these molecules were further analyzed using global and local descriptors by extracting the information about their biological reactivity for designing new medical drugs [70–74].

2. Results and Discussion

2.1. Analysis of MIC against *C. albicans*

The inhibitory potential of pyrrolo [1, 2-a]quinoline derivatives targeted against *C. albicans* were observed after 24 h of incubation. The derivatives BQ-06, 07 and 08 show the highest minimum inhibitory concentrations (MICs) at 0.4 µg/mL, whereas BQ-01, 03, and 05 have MICs of 0.8 µg/mL. Further, the BQ-04 derivative possesses an MIC of 1.6 µg/mL, followed by BQ-12 which causes inhibition of growth of *C. albicans* at 12.5 µg/mL (Table 1).

Table 1. Minimum inhibitory concentration of pyrrolo[1,2-a]quinoline derivatives against *C. albicans*.

Sample	MIC (µg/mL)
BQ-01	0.8
BQ-02	12.5
BQ-03	0.8
BQ-04	1.6
BQ-05	0.8
BQ-06	0.4
BQ-07	0.4
BQ-08	0.4

2.2. Molecular Docking

Binding orientation of pyrrolo[1,2-a] quinoline on target proteins 2H6T, 3N9K and 5TZ1 from *C. albicans* were assessed by molecular docking analysis. Out of the eight pyrrolo[1, 2-a] quinoline derivatives, BQ-01, 03, 05, and 07 were used for molecular docking analysis. These molecules possess common methyl ester groups at the second and third positions. However, BQ-02, 04, 06 and 08 consist of a common hydrogen group at the second position and ethyl ester at third position. The results obtained for docking between the macromolecule and ligand show eight poses of the ligand molecule that is docked at the macromolecule (protein). The confirmation of pose consisting of the least binding affinity was saved in .pdb format and their interactions were studied using Pymol software (The PyMOL Molecular Graphics System, Version 2.0 Schrödinger, LLC). The amino acid pocket residues of the macromolecule interaction with the ligand were analyzed for the bonded (H-bonds) and nonbonded interactions (hydrophobic interactions) and were later visualized by using Pymol software. The formation of the number of hydrogen bonds (H-bonds) forming amino acid residues and binding free energy of the interaction between protein targets and ligands obtained are shown in Table 2. Further, the number of hydrogen bonds formed were identified for the ligand molecules BQ-03, BQ-05, and BQ-07 (6, 5, and 6 hydrogen bonds, respectively) against *C. albicans* protein 2H6T, which shows a stronger binding interaction than the drug candidate (four hydrogen bonds). The H-bond forming amino acid residues between the ligand molecules BQ-01, 03, 05, and 07 and the protein target 2H6T were identified as THR-221 and THR-222. Further, BQ-03 and 05 also actively interact with THR-221 and THR-222 along with GLY-220, whereas BQ-07

interacts with THR-221 and THR-222 along with VAL-12. Moreover, these molecules exhibit potential binding affinity to the amino acid residues, which possess different interaction sites compared to that of the therapeutic antifungal drug fluconazole. However, in the cases of *C. albicans* proteins 3N9K and 5TZ1, the number of hydrogen bonds formed with the ligands were less than or equal to fluconazole. Interestingly, the H-bond forming amino acid residues identified by the interaction analyses were different from that of fluconazole, which indicates novel binding interaction of the ligand molecules to the macromolecular target. These results offers pyrrolo[1,2-a]quinoline analogues as putative novel targets against drug-resistant *C. albicans* fungal pathogens.

Table 2. The details of the H-bond formation and binding free energy.

Sl No	Macromolecule/Protein Target	Ligand/Small Molecule	Number of Hydrogen Bonds	H-Bond Forming Amino Acid Residues	ΔG (Kcal/mol)
1	2H6T	Drug	4	SER-13, ASP-86, ASP-120 and GLN-121	−7.5
		BQ-01	3	THR-221 and THR-222	−6.5
		BQ-03	6	THR-221, THR-222 and GLY-220	−7.4
		BQ-05	5	THR-221, THR-222 and GLY-220	−7.2
		BQ-07	6	THR-221, THR-222 and VAL-12	−6.8
2	3N9K	Drug	3	ASP-145, LEU-304 and ASN-305	−7.8
		BQ-01	2	PHE-144 and ASN-146	−9.4
		BQ-03	2	ASN-146	−9.7
		BQ-05	3	ASN-146 and TYR-317	−9.4
		BQ-07	2	ASN-146	−9.2
3	5TZ1	Drug	4	TYR-132, PHE-463 and ARG-469	−7.2
		BQ-01	2	TYR-132	−8.9
		BQ-03	2	TYR-132	−8.1
		BQ-05	1	TYR-132	−8.6
		BQ-07	2	TYR-132	−8.7

Further, the ligands and macromolecular targets (3N9K and 5TZ1) possess stronger binding free energy than fluconazole, as shown in Table 2. Among the tested ligands, BQ-03 shows binding free energies of −7.4, −9.7 and −9.1 kcal/mol against 2H6T, 3N9K and 5TZ1, respectively. The binding interaction between target proteins 3N9K and 5TZ1 and all the tested ligands (BQ-01, BQ-03, BQ-05, and BQ-07) showed ΔG values that are higher than fluconazole and it reveals that these compounds possess a stronger affinity towards the protein targets 3N9K and 5TZ1 than the drug, indicating that the interaction between the ligand molecule and the protein is possible and thermodynamically favorable. Further, a high number of hydrogen bonds were formed with ligand-2H6T interactions; however, strong binding affinity in terms of binding free energy was observed with ligand-3N9K, and ligand-5TZ1 interactions. These results show the presence of nonbonded interactions along with hydrogen bonds in ligand-3N9K and ligand-5TZ1 interactions. The strong binding interaction of ligands BQ-01, 03, 05, and 07, compared to fluconazole, to protein targets 3N9K and 5TZ1, are a good platform for further development of a novel drug target against *C. albicans*. The free energy change upon binding of protein–ligand interaction has been shown as follows:

Fluconazole interacted with 2H6T with a binding affinity of −7.5 kcal/mol, while it showed −7.8 and −7.2 kcal/mol binding energy when interacting with 3N9K and 5TZ1, respectively.

The BQ-01 ligand interacted with 2H6T with a binding affinity of −6.5 (kcal/mol), while it showed −9.4 (kcal/mol) and −8.9 (kcal/mol) binding energies when interacting with 3N9K and 5TZ1, respectively.

The BQ-03 ligand interacted with 2H6T with a binding affinity of −7.4 (kcal/mol), while it showed −9.7 (kcal/mol) and −9.1 (kcal/mol) binding energies when interacting with 3N9K and 5TZ1, respectively.

The BQ-05 ligand interacted with 2H6T with a binding affinity of -7.2 (kcal/mol), while it showed -9.4 (kcal/mol) and -8.6 (kcal/mol) binding energies when interacting with 3N9K and 5TZ1, respectively.

The BQ-07 ligand interacted with 2H6T with a binding affinity of -6.8 (kcal/mol), while it showed -9.2 (kcal/mol) and -8.7 (kcal/mol) binding energies when interacting with 3N9K and 5TZ1, respectively.

Further, the docking result confirms that the drug fluconazole (Figure 2) or ligand molecules BQ-01 (Figure 3), 03 (Figure 4), 05 (Figure 5) and 07 (Figure 6) were held in the active pocket of the *C. albicans* fungal proteins 2H6T, 3N9K or 5TZ1, respectively.

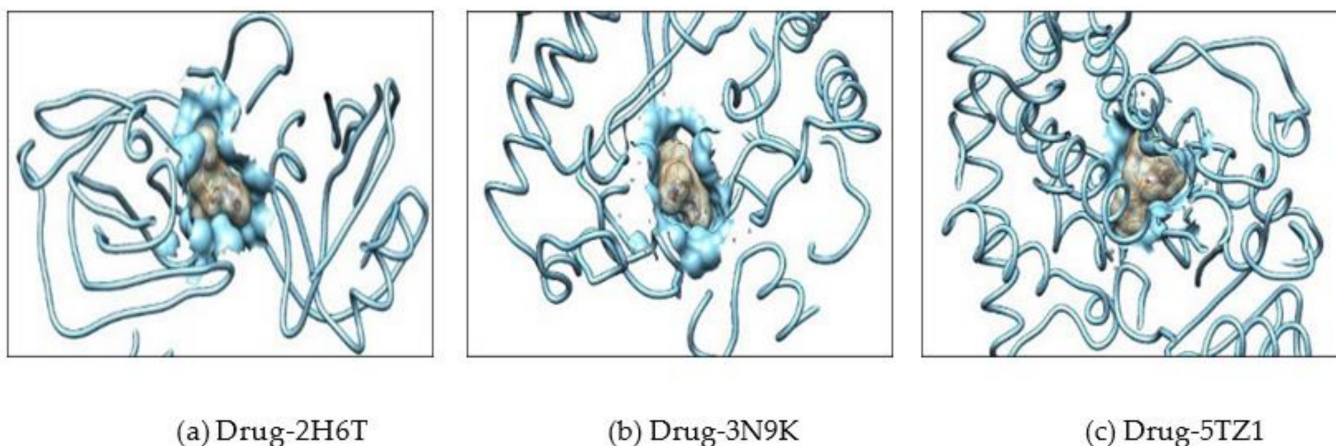


Figure 2. Showing interaction of the drug (fluconazole) molecule which completely fit into the hydrophobic pocket of the *C. albicans* fungal proteins—(a) 2H6T, (b) 3N9K and (c) 5TZ1.

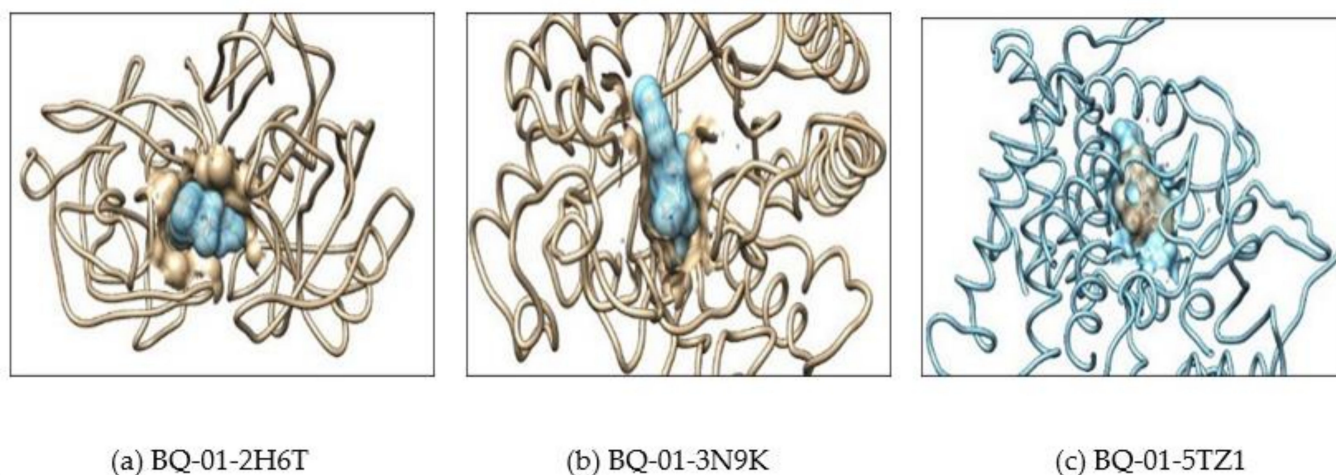


Figure 3. (a) Showing interaction of the BQ-01 molecule which completely fit into the hydrophobic pocket of the *C. albicans* fungal proteins—2H6T, (b) 3N9K and (c) 5TZ1.

2.3. Determination of the Conceptual DFT Reactivity Descriptors of the Molecules and their Related Pharmacokinetics

The determination of conformers of the molecules considered in the current study was performed by utilizing various software described elsewhere, as described in Section 3.5 [75–91]. Further, the results obtained from the model chemistry consider the MN12SX screened-exchange density function [81] together with the Def2TZVP basis set [82,83], and in all cases the charge of the molecules was equal to zero while the radical anion and cation were considered in the doublet spin state.

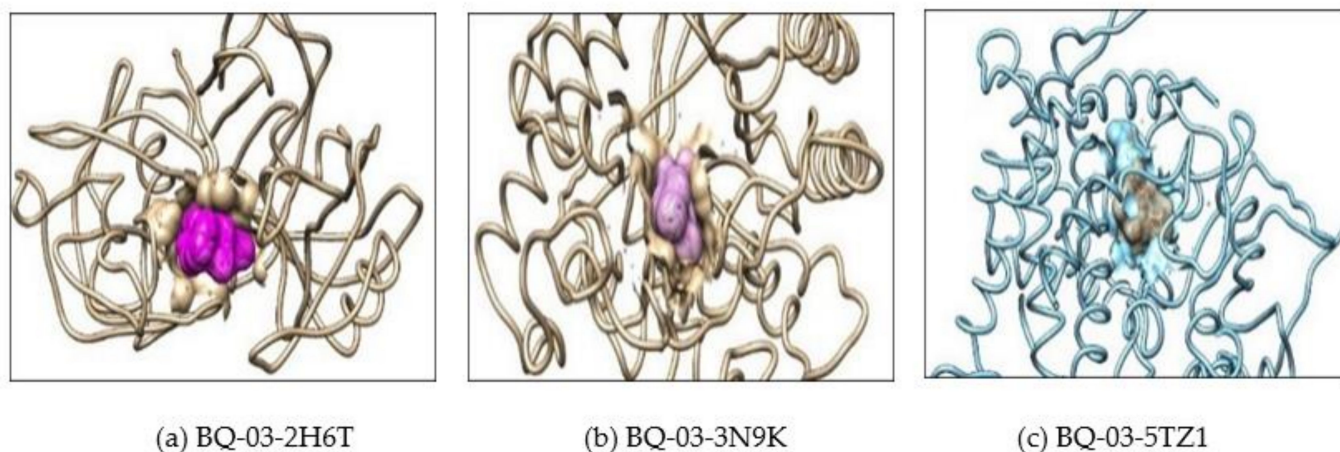


Figure 4. Showing interaction of the BQ-03 molecule which completely fit into the hydrophobic pocket of the *C. albicans* fungal proteins—(a) 2H6T, (b) 3N9K and (c) 5TZ1.

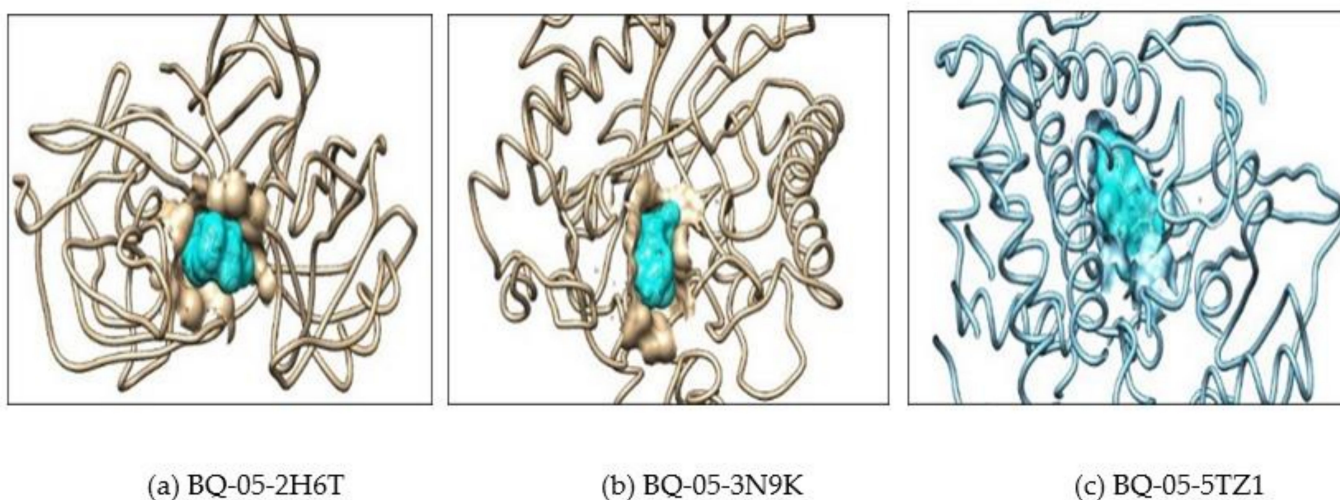


Figure 5. Showing interaction of the BQ-05 molecule which completely fit into the hydrophobic pocket of the *C. albicans* fungal proteins—(a) 2H6T, (b) 3N9K and (c) 5TZ1.

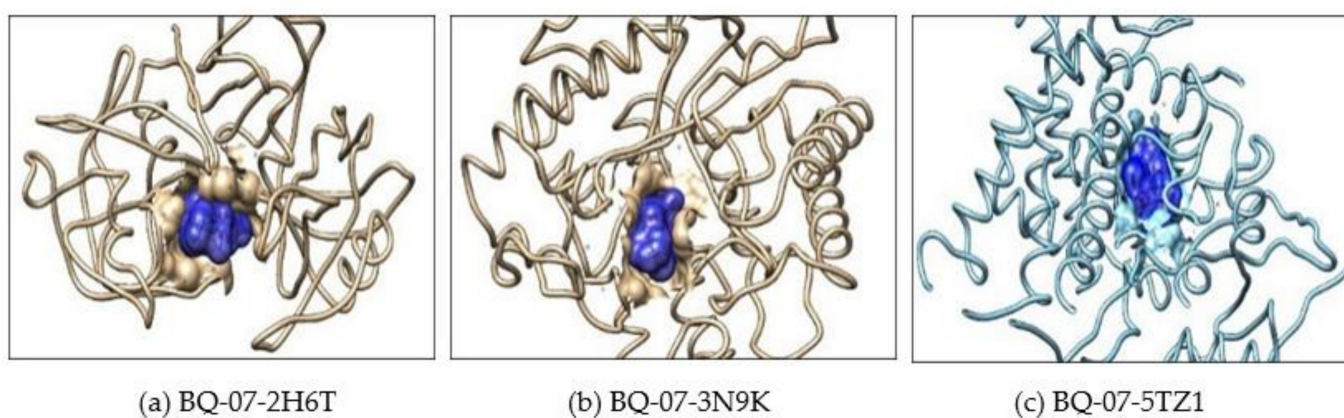


Figure 6. Showing interaction of the BQ-07 molecule which completely fit into the hydrophobic pocket of the *C. albicans* fungal protein—(a) 2H6T, (b) 3N9K and (c) 5TZ1.

Further, assumption of the goodness of a given density functional can be estimated by comparing the results with the experimental values that are being reproduced or with the

results that can be obtained through post Hartree–Fock calculations such as MP2, MP4 or CCSD. However, this is not always possible due to the lack of experimental results for the molecular systems that are being studied or the large size of the molecules that keep some accurate methodologies computationally practical. For this reason, we have developed a protocol named Koopmans in DFT (KID) [92–94], which is an attempt to validate a given density functional in terms of its internal coherence. Within the KID protocol, four descriptors have been defined where it has been shown that there is a connection between those descriptors and the simplest conformity to the theorem of Koopmans or the Ionization Energy theorem, which is its equivalent within the Generalized Kohn–Sham (GKS) version of DFT, by connecting the electronic energy of the Highest Occupied Molecular Orbital (HOMO)—that is, ε_H —with the negative of the ionization energy, I , and the electronic energy of the Lowest Unoccupied Molecular Orbital (LUMO)—that is ε_L —with the negative of the Electron affinity, A , giving rise to $J_I = |\varepsilon_H + E_{gs}(N - 1) - E_{gs}(N)|$, $J_A = |\varepsilon_L + E_{gs}(N) - E_{gs}(N - 1)|$, and $J_{HL} = \sqrt{J_I^2 + J_A^2}$, where $E_{gs}(N)$, $E_{gs}(N - 1)$ and $E_{gs}(N + 1)$ represents the ground state energy of the neutral molecule, of the radical cation and the radical anion, respectively, in the geometry of the neutral molecule. An additional descriptor, ΔSL , was designed [92–94] to help in the verification of the accuracy of the KID approximation by comparing the HOMO energy of the radical anion with the energy of the LUMO of the neutral species. Although the Koopmans complaint behavior of the MN12SX density functional has been proven previously for the case of peptides [92–94], we think that it is worth performing a further validation for the case of the molecules considered in the present study.

As we have shown in our previous research [85–90,95], the KID procedure is also valid in the presence of water as the solvent and represents an advantage over the use of the vertical I and A for the calculation of the global descriptors because it avoids the separate calculation of the radical cation and anion which could be difficult for molecules of the size considered here. It has been shown by Frau and Glossman-Mitnik [69,84–90,95] that the HOMO and LUMO energies obtained with the MN12SX/Def2TZVP/H₂O model chemistry allow the verification of the KID procedure—that is, rendering an approximate Koopmans behavior. All the calculated molecules are neutral—that is, they have a charge equal to zero—and these optimized structures were considered for the estimation of the energies of the cation and anion radicals because the definitions of the conceptual DFT descriptors have been derived at constant external potential [72–74,96,97].

The HOMO, LUMO and Singly Occupied Molecular Orbital (SOMO, which is equivalent to the HOMO of the radical anion) orbital energies, HOMO–LUMO gap and the KID descriptors (all in eV) tested in the verification of the Koopmans-like behavior of the MN12SX density functional for the new BQ molecules are shown in Table 3, while the calculated values for these global reactivity descriptors using the MN12SX/Def2TZVP/H₂O model chemistry and the KID procedure are displayed in Table 4.

Table 3. Highest Occupied Molecular Orbital (HOMO), Lowest Unoccupied Molecular Orbital (LUMO) and Singly Occupied Molecular Orbital (SOMO) orbital energies, HOMO–LUMO gap and the Koopmans in DFT (KID) descriptors (all in eV) tested in the verification of the Koopmans-like behavior of the MN12SX density functional for the new BQ molecules.

	HOMO	LUMO	SOMO	H-L Gap	J_I	J_A	J_{HL}	ΔSL
BQ-01	−5.9207	−2.3551	−2.5429	3.5655	0.001	0.103	0.103	0.188
BQ-02	−5.8513	−2.2455	−2.5712	3.4058	0.008	0.061	0.062	0.126
BQ-03	−5.9443	−2.6011	−2.7470	3.3432	0.003	0.081	0.081	0.146
BQ-04	−5.9158	−2.5666	−2.6830	3.3492	0.008	0.058	0.058	0.117
BQ-05	−5.9634	−2.9456	−3.0507	3.0177	0.003	0.056	0.056	0.105
BQ-06	−5.9552	−2.7737	−2.8771	3.1816	0.008	0.052	0.052	0.103
BQ-07	−5.9381	−2.5225	−2.6975	4.4156	0.002	0.096	0.096	0.175
BQ-08	−5.9073	−2.5239	−2.6458	3.3835	0.008	0.060	0.061	0.122

Table 4. Global reactivity descriptors for the new BQ molecules: electronegativity (χ), hardness (η), electrophilicity (ω) (all in eV), softness S (in eV^{-1}), nucleophilicity N, electrodonating Power (ω^-), electroaccepting Power (ω^+) and net electrophilicity ($\Delta\omega^\pm$) (also in eV).

	χ	η	ω	S	N	ω^-	ω^+	$\Delta\omega^\pm$
BQ-01	4.1379	3.5655	2.4011	0.2805	2.8718	7.0940	2.9561	10.0501
BQ-02	4.1484	3.4058	2.5264	0.2936	2.9412	7.3399	3.1916	10.5315
BQ-03	4.2727	3.3432	2.7304	0.2991	2.8482	7.8060	3.5333	11.3393
BQ-04	4.2412	3.3492	2.6854	0.2986	2.8767	7.7006	3.4595	11.1601
BQ-05	4.4545	3.0177	3.2877	0.3314	2.8291	8.9912	4.5367	13.5279
BQ-06	4.3644	3.1816	2.9936	0.3143	2.8373	8.3682	4.0037	12.3719
BQ-07	4.2303	3.4156	2.6197	0.2928	2.8544	7.5679	3.3377	10.9056
BQ-08	4.2156	3.3835	2.6262	0.2956	2.8852	7.5716	3.3560	10.9277

It can be seen from the results in Table 1 that the descriptors considered for the estimation of the goodness of the selected density functional through the KID procedure are very close to zero for all the studied molecules, providing an accurate justification for the choice of the MN12SX/Def2TZVP/H2O model chemistry employed for the computational determinations in this study.

As a complement to these global reactivity descriptors that arise from conceptual DFT, Domingo and his collaborators [98] proposed a nucleophilicity index (N) (not to be confused with the number of electrons) through the consideration of the HOMO energy obtained through the KS scheme with an arbitrary shift of the origin taking the molecule of tetracyanoethylene (TCE) as a reference. On the basis of the previous definition and the scale established by these authors [98], and the results presented in Table 4, it can be concluded that all the molecules considered in this study can be regarded as moderate nucleophiles.

Next, QSAR analysis was carried out on the molecular properties of the new BQ molecules, such as ΔG of solvation, molecular weight, Log P, total polar surface area (TPSA), and molecular volume, using Molinspiration software. The predicted parameters are shown in Table 5.

Table 5. Predicted parameters useful for QSAR analyses for the new BQ molecules: ΔG of solvation (in Kcal/mol), Molecular Weight (MW), Partition Coefficient (logP), Total Polar Surface Area (TPSA) (\AA^2) and Molecular Volume (\AA^3).

	ΔG of Solvation	MW	log P	TPSA	Molecular Volume
BQ-01	−12.66	496.31	5.07	83.33	380.28
BQ-02	−9.69	438.28	5.31	57.02	335.75
BQ-03	−10.91	500.73	5.69	74.10	368.27
BQ-04	−8.46	442.70	5.93	47.79	323.74
BQ-05	−12.81	491.30	4.76	97.89	371.59
BQ-06	−10.64	433.26	5.00	71.58	327.06
BQ-07	−11.22	466.29	5.01	74.10	354.73
BQ-08	−8.45	408.25	5.25	47.79	310.20

The results presented in Table 5 can be better understood if a graphical representation of these physicochemical properties displays in the form of what is known as a bioavailability radar, where six physicochemical properties are considered: lipophilicity, size, polarity, solubility, flexibility, and saturation. Each descriptor must fall entirely within the physicochemical range depicted in the pink area of the radar plot of the molecule to be considered drug-like. These results are presented in Figure 7.

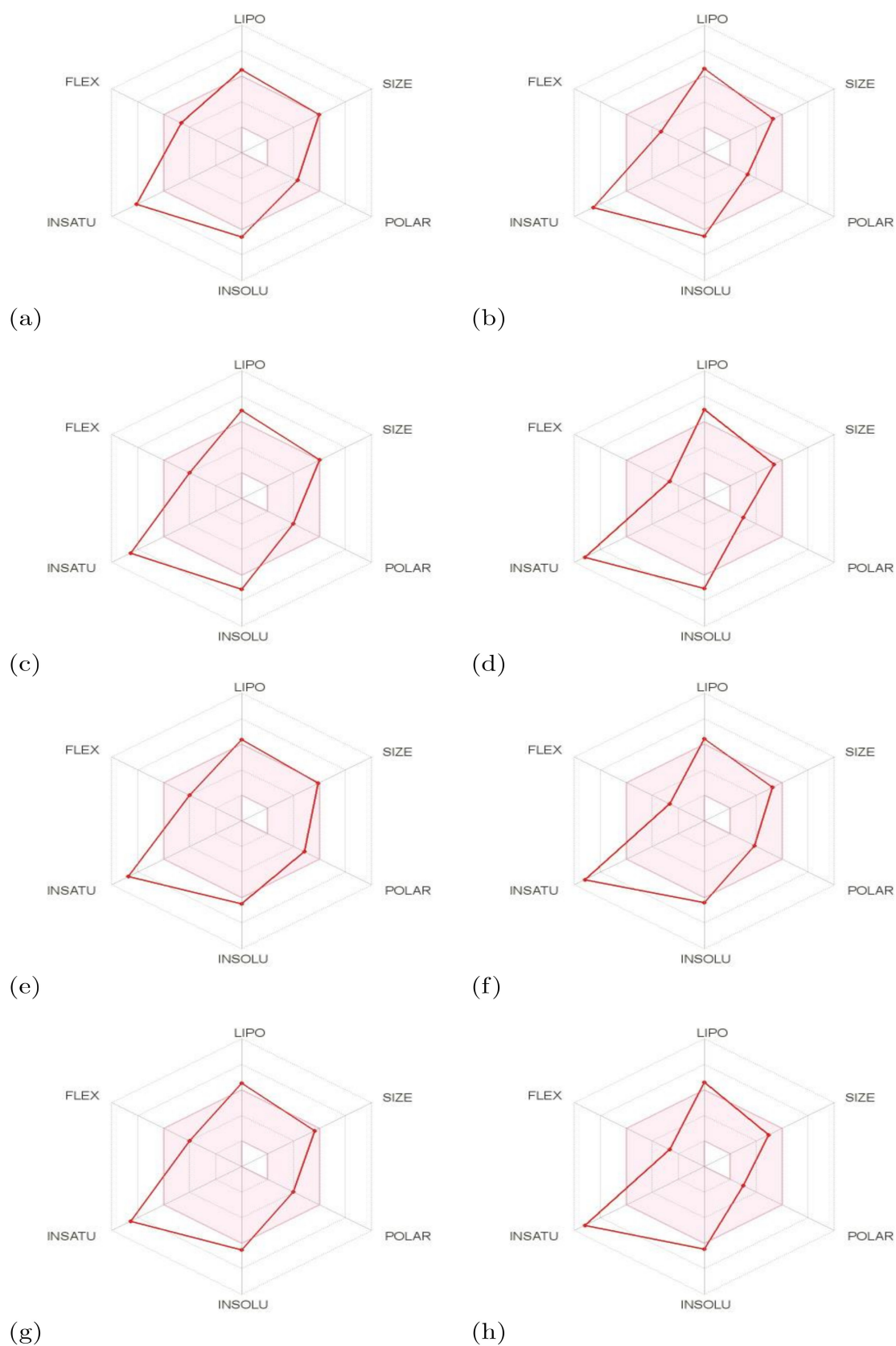


Figure 7. Bioactivity radars of the (a) BQ-01, (b) BQ-02, (c) BQ-03, (d) BQ-04, (e) BQ-05, (f) BQ-06, (g) BQ-07, and (h) BQ-08 molecules.

Next, a web tool known as SwissTargetPrediction for efficient prediction of protein targets of small molecules was considered for the determination of the potential bioactivity of the molecules considered in this study [99]. The associated website allows the estimation of the most probable macromolecular targets of a small molecule assumed as bioactive. The prediction confirms that a combination of 2D and 3D similarity with a library of 370,000 known actives on more than 3000 proteins from three different species, as shown in Figure 8.

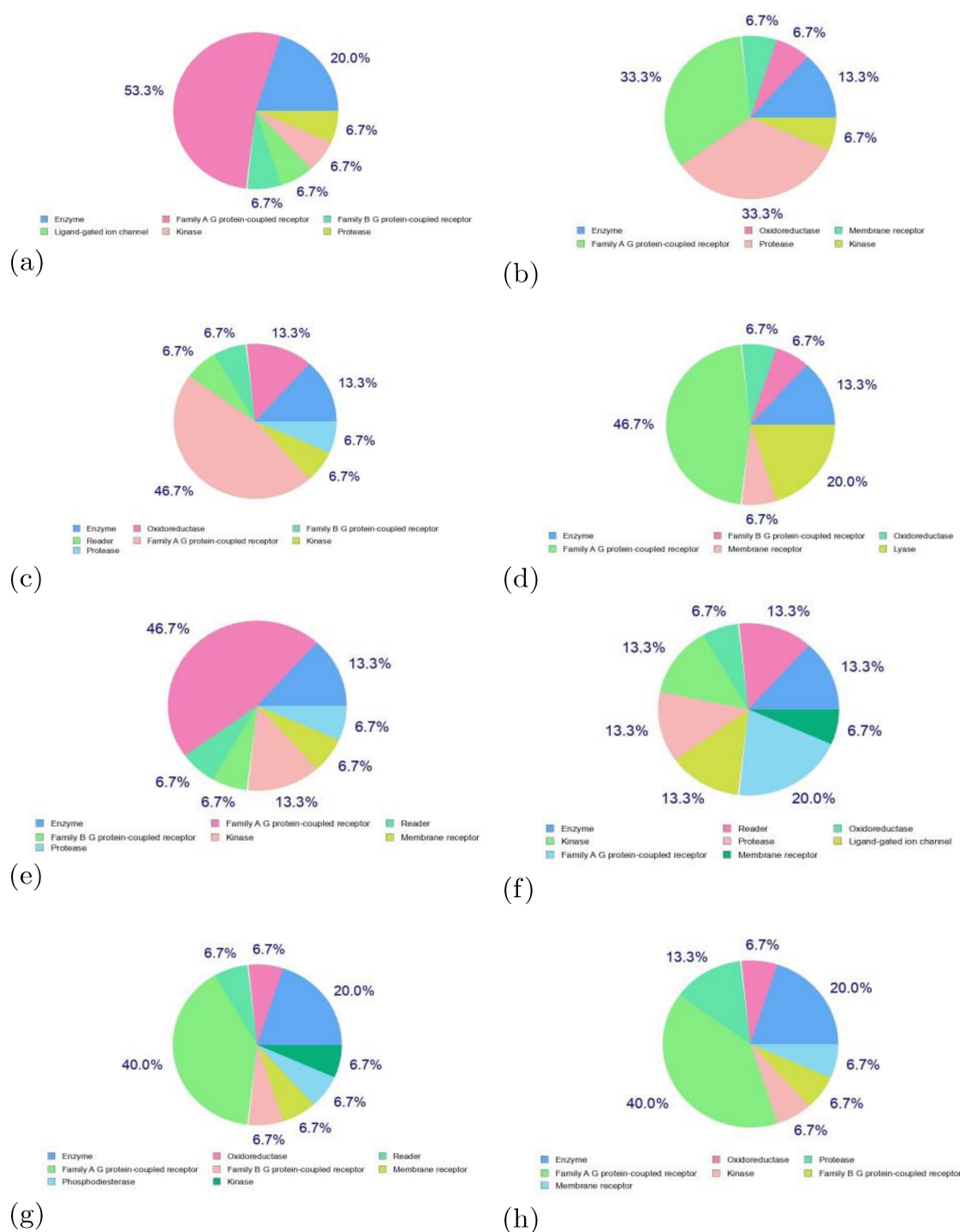


Figure 8. Predicted biological targets of the (a) BQ-01, (b) BQ-02, (c) BQ-03, (d) BQ-04, (e) BQ-05, (f) BQ-06, (g) BQ-07, and (h) BQ-08 molecules.

During the development process of a new drug, it is very important to know the possible fate of a therapeutic compound in an organism, a process that is known as pharmacokinetics. This can be achieved by analyzing the associated effects in the form of individual indices that involve Absorption, Distribution, Metabolism, and Excretion (ADME) parameters. These parameters can be obtained by using computer models that can be alternatives to the experimental procedures for their determination. In this work, some ADME parameters were estimated with the aid of the SwissADME software that is available online [100], and the results are presented in Table 6.

Table 6. Absorption, Distribution, Metabolism, and Excretion (ADME) parameters related to the pharmacokinetics of the new BQ molecules.

	BQ-01	BQ-02	BQ-03	BQ-04
GI absorption	HIGH	HIGH	HIGH	HIGH
BBB permeant	NO	YES	NO	YES
P-gp substrate	NO	NO	NO	NO
CYP1A2 inhibitor	NO	YES	NO	YES
CYP2C19 inhibitor	YES	YES	YES	YES
CYP2C9 inhibitor	YES	YES	YES	YES
CYP2D6 inhibitor	NO	NO	NO	NO
CYP3A4 inhibitor	NO	NO	NO	NO
Log $K_p/cm\ s^{-1}$ (skin permeation)	−5.15	−4.69	−4.71	−4.26
	BQ-05	BQ-06	BQ-07	BQ-08
GI absorption	HIGH	HIGH	HIGH	HIGH
BBB permeant	NO	NO	NO	YES
P-gp substrate	NO	NO	NO	NO
CYP1A2 inhibitor	NO	YES	YES	YES
CYP2C19 inhibitor	YES	YES	YES	YES
CYP2C9 inhibitor	YES	YES	YES	YES
CYP2D6 inhibitor	NO	NO	NO	NO
CYP3A4 inhibitor	NO	NO	NO	NO
Log $K_p/cm\ s^{-1}$ (skin permeation)	−5.30	−4.85	−4.95	−4.49

3. Materials and Methods

3.1. Analysis of Minimum Inhibitory Concentration against *C. albicans*

The minimum inhibitory concentrations (MICs) were calculated according to the proposed protocol by Schwälbe et al. (2007). Briefly, 20 μ L of each pyrrolo[1,2-a]quinoline derivative from the stock solution was added into the first tube containing 380 μ L of brain heart infusion (BHI, HiMedia) broth to achieve 100 μ g/mL concentration. Then, 200 μ L of each derivative was serially diluted starting from 100 to 0.2 μ g/mL (in total of 9 dilutions i.e., 10^{-1} to 10^{-9}) in BHI broth separately. From the stock solution, 5 μ L of inoculum containing pure culture of *C. albicans* (ATCC no. 10231; 16 μ g/mL) was added into 2ml of BHI broth and later, mixed with the serially diluted tubes containing pyrrolo[1,2-a]quinoline derivatives. The standard value for fluconazole in the MIC tests was 30 μ g. The tubes were later incubated for 24 h and observed for appearance of turbidity.

3.2. Selection of Protein

The synthesized ligand compounds act as inhibitors that reduces the growth of *C. albicans* by interacting with the pathogenic proteins such as secreted aspartic protease 3 (SAP3), fungal cell surface protein (β -glucanase) and the sterol 14- α demethylase receptors as reported elsewhere. In this study, the protein targets identified are SAP protein (SAP-3), surface protein and sterol 14- α demethylase, which were used to carry out the in silico analyses. The required crystal structures of the above-mentioned proteins of *C. albicans* were selected and extracted from an online Protein Data Bank (PDB) database based

on their structures, functions and resolutions. The PDB IDs for the SAP-3 protein, β -glucan protein and sterol 14- α demethylase are 2H6T, 3N9K and 5TZ1, respectively, and a further file was secured in pdb format for further analysis. The molecular visualization of these proteins was accomplished by utilizing Chimera software [101] and required modifications were applied to remove the nonstandard amino acids or the pre-existing ligands and the water molecules attached with the protein structure (Figure 9a–c). Next, the stability of the protein structures was assessed using RAMPAGE [102], which displays the percentage of amino acid residues present in the allowed and favored regions. The proteins with more than 96% of residues in the favored and less than 2% of residues in the allowed regions were selected for further in silico analysis. Based on the desirable value obtained, the selected pathogenic proteins for further molecular interaction and docking analysis were macromolecules.

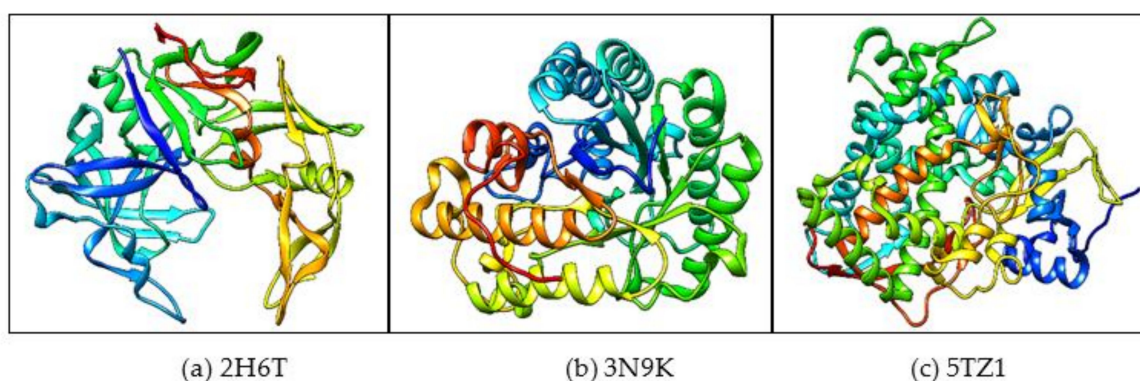


Figure 9. The Protein Data Bank (PDB) structure of the three selected proteins in ribbon preset (a) 2H6T, (b) 3N9K and (c) 5TZ1. The secondary structures of *C. albicans* fungal proteins are represented by blue, red, orange, green and yellow.

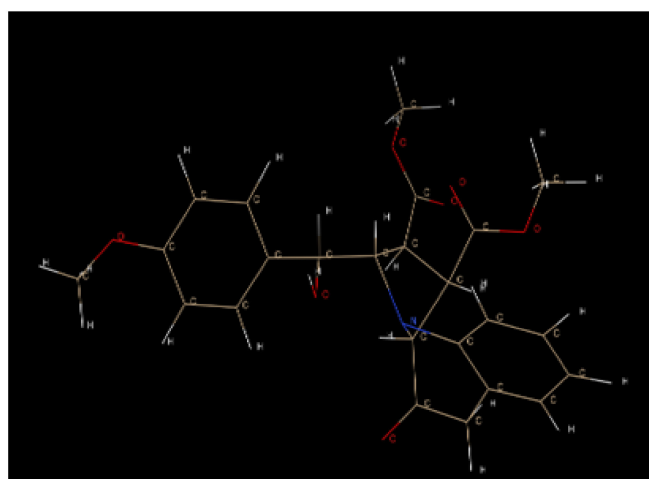
3.3. Small Molecule Optimization

The structures of small molecules (BQ-01, BQ-03, BQ-05 and BQ-07) used as molecular targets against *C. albicans* were saved in the pdb format for further in silico analysis. For preparation of ligand, we utilized three different tools: 1. ChemsKetch software [103], used here to sketch the small molecules and the resulted output file was saved in chemical markup language (cml) format; 2. OpenBabel software [104], utilized for conversion of the 2D structure cml file obtained from ChemsKetch to pdb format, thereby generating the 3D coordinates; 3. Chimera software, utilized for visualization of resultant file obtained from OpenBabel (Figure 10a–d). The small molecules referred to as ligands in the above mentioned file format were subjected to further in silico molecular interaction analysis.

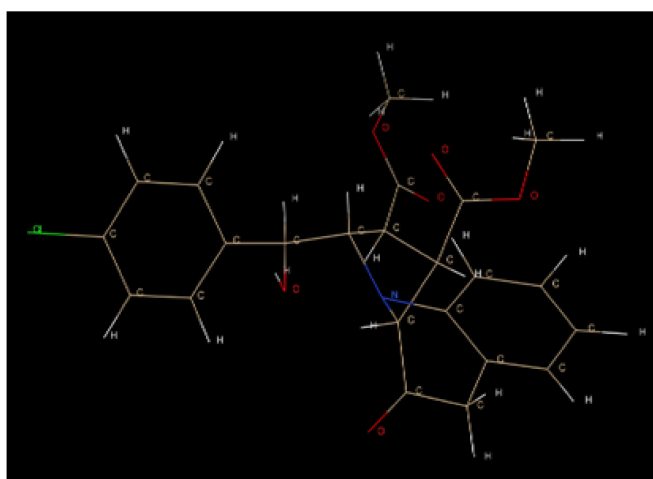
Next, comparative analyses were carried out to compare the binding interactions results from the synthesized ligands and the pre-existing drug against the *C. albicans* surface and SAP-3 receptors. The .sdf format file of the FDA approved drug file was taken from the online database PubChem. The mandatory .pdb 3D format file for the in silico docking analyses is essential; hence, the .sdf format of the drug was converted to .pdb format using OpenBabel software and visualized using Chimera software (Figure 11).

3.4. In Silico Molecular Interaction and Docking

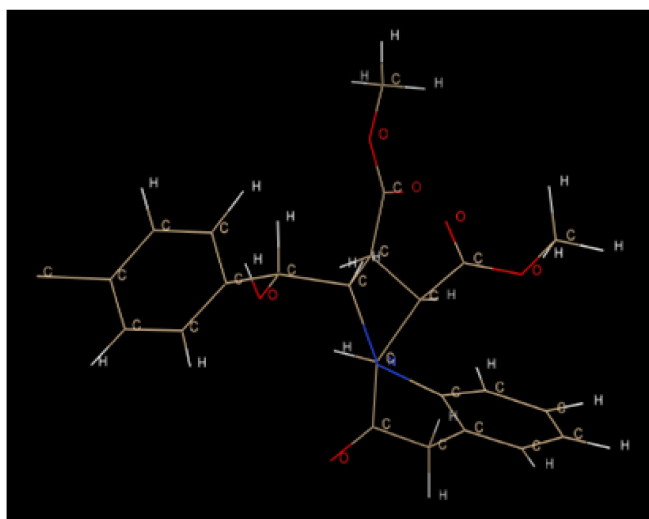
The molecular interaction of the small molecules and their inhibitory potential against the *C. albicans* fungal proteins were studied using in silico molecular docking. Here, the molecular docking interactions were between the selected proteins from PDB against the optimized small molecules using PyRx software [105]. The respective macromolecule and the ligands were loaded onto the software and the active site residues were selected and grid box was generated around the selected amino acid residues. The docking results was carried out using a genetic algorithm. Moreover, the interaction achieved eight docking confirmations.



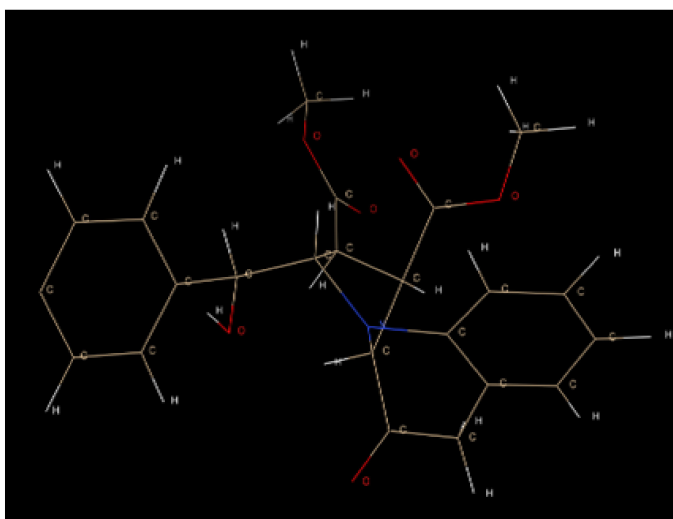
(a) BQ-01



(b) BQ-03



(c) BQ-05



(d) BQ-07

Figure 10. The 3-dimensional structure of the ligand molecules visualized using Chimera: (a) BQ-01, (b) BQ-03, (c) BQ-05 and (d) BQ-07.

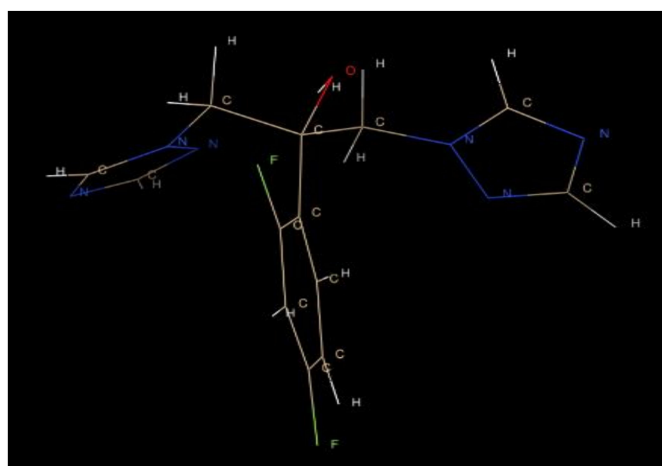


Figure 11. The 3-dimensional structure of the drug (fluconazole) visualized using Chimera.

3.5. Conceptual DFT Reactivity Descriptors of the Molecules and Their Related Pharmacokinetics

The determination of the conformers of the molecules considered in the current study was performed by resorting to MarvinView 17.15, which is available from ChemAxon (<http://www.chemaxon.com>, accessed on 6 October 2020), by carrying out molecular mechanics calculations through the overall MMFF94 force field [75–79]. This was followed by a new geometry optimization and frequency calculation by means of the Density Functional Tight Binding (DFTBA) methodology [80]. This last step was required to verify the absence of imaginary frequencies to assess for the minimum stability of the optimized structures-in the energy landscape. The electronic properties and the chemical reactivity descriptors of the studied molecules involved the use of MN12SX/Def2TZVP/H2O [81–83] model chemistry on the previously optimized molecular structures because it has been shown that it allows the verification of the “Koopmans in DFT” (KID) procedure [69,84–90] with the aid of the Gaussian09 software [80] and the SMD solvation model [91].

With the aid of the KID technique and the finite difference approximation [69,84–90,95], the following expressions can be used to define the global reactivity descriptors [72–74,96,97]:

Electronegativity

$$\chi = -\frac{1}{2}(I + A) \approx \frac{1}{2}(\varepsilon_L + \varepsilon_H) \quad (1)$$

Chemical Hardness

$$\eta = (I - A) \approx (\varepsilon_L - \varepsilon_H) \quad (2)$$

Global Electrophilicity

$$\omega = \frac{\chi^2}{2\eta} = \frac{(I + A)^2}{4(I - A)} \approx \frac{(\varepsilon_L + \varepsilon_H)^2}{4(\varepsilon_L - \varepsilon_H)} \quad (3)$$

Electrodonating Power

$$\omega^- = \frac{(3I + A)^2}{16(I - A)} \approx \frac{(3\varepsilon_H + \varepsilon_L)^2}{16\eta} \quad (4)$$

Electroaccepting Power

$$\omega^+ = \frac{(I + 3A)^2}{16(I - A)} \approx \frac{(\varepsilon_H + 3\varepsilon_L)^2}{16\eta} \quad (5)$$

Net Electrophilicity

$$\Delta\omega^\pm = \omega^+ - (-\omega^-) = \omega^+ - \omega^- \quad (6)$$

where, as mentioned, ε_H and ε_L are the energies of the HOMO and LUMO, respectively.

After analyzing KID descriptors, The SMILES notation of all the studied compounds were fed into the online Molinspiration software from Molinspiration Cheminformatics (<http://www.molinspiration.com>, accessed on 6 October 2020) for the calculation of the molecular properties (ΔG of Solvation, molecular weight, Log P, total polar surface area (TPSA), and molecular volume). The bioactivity scores were compared to those obtained using other software such as MolSoft from Molsoft L.L.C. (<http://molsoft.com/mprop/>, accessed on 6 October 2020) and ChemDoodle Version 9.02 from iChemLabs L.L.C. (<http://www.chemdoodle.com>), accessed on 6 October 2020.

4. Conclusions

The study shows novel pyrrolo[1,2-a]quinoline derivatives as putative drug targets of *C. albicans*. Here, in vitro screening of novel analogue derivatives against *C. albicans* fungal pathogen displayed inhibitory potentials of 75-fold for BQ-06, 07, and 08, and 37.5-fold for BQ-01, 03, and 05, followed by 18.75-fold for BQ-04, and 2.4-fold for BQ-02, in comparison to the standard antifungal fluconazole. Further, in silico molecular docking prediction of

the ligand molecules BQ-01, 03, 05 and 07 compared to the drug alone exhibited strong hydrogen binding interactions with the regulating *C. albicans* protein β -glucan (3N9K), which demonstrates thermodynamically favorable conditions. Furthermore, these compound shows high binding energies ranging from -6.5 to -9.7 kcal/mol. However, based on the chemical structure, BQ-01, 03, 05 and 07 consist of methyl ester groups at the second and third positions compared to that of only one methyl ester at the third position, which is the case for BQ-02, 04, 06 and 08. Furthermore, BQ-01, 03, 05 and 07 possess a two-electron donor group, due to their effective interaction with *C. albicans* fungal proteins, which inhibits their growth compared to the single-electron donor groups present at the third positions of BQ-02, 04, 06 and 08. In addition, the determination of the chemical reactivity descriptors that arise from conceptual DFT allowed us to quantify the different values for the chemical reactivity of the studied molecules. Further, QSAR parameters, biological radars, exploration of possible targets and the pharmacokinetics of the systems suggested that compounds BQ-01, 03, 05 and 07 have good drug-like properties. In conclusion, the analyzed parameters can be useful in complementing the experimental data as the starting point for the development of new antifungal therapeutic drugs.

Author Contributions: Conceptualization, B.P., S.C. and K.K.M.-N.; methodology, S.C., V.U., C.S., S.P., S.P.K., M.C., J.O.-C., J.F., N.F.-H., A.I.B. and D.G.-M.; software, S.P., N.F.-H. and D.G.-M.; validation, S.C., K.K.M.-N., B.P. and D.G.-M.; formal analysis, S.C., K.N.V., G.B., Jayadev and B.P.N.; investigation, K.K.M.-N., V.U., S.C., C.S., M.C., M.M.M., J.O.-C., J.F., N.F.-H., A.I.B. and D.G.-M.; resources, K.N.V., A.A.A.-K., A.S. and A.M.E.; data curation, S.C., V.U., C.S., S.P., S.P.K. and M.M.M.; writing—original draft preparation, B.P., S.C., K.K.M.-N. and D.G.-M.; writing—review and editing, K.K.M.-N., M.C., G.B., Jayadev and B.P.N.; visualization, C.S., S.P. and S.P.K.; supervision, B.P., S.C. and K.K.M.-N.; project administration, B.P., S.C. and K.K.M.-N.; funding acquisition, B.P., S.C., K.K.M.-N., N.F.-H., D.G.-M., R.V., A.A.A.-K., A.S. and A.M.E. All authors have read and agreed to the published version of the manuscript.

Funding: The authors are grateful to the Deanship of Scientific Research, King Saud University, for funding through Vice Deanship of Scientific Research Chairs.

Institutional Review Board Statement: Not applicable.

Informed Consent Statement: Not applicable.

Acknowledgments: The authors acknowledge the Rani Channamma University, Belagavi, for providing laboratory facilities and JSS Academy of Higher Education and Research, Mysore, for carrying out antimicrobial activity and in silico molecular docking experiments. Further, DGM is a Visiting Professor at the Universitat de les Illes Balears from whose support is gratefully acknowledged. Moreover, N.F.-H. and D.G.-M. would like to thank CIMAV and CONACYT for partial support. The authors are grateful to the Deanship of Scientific Research, King Saud University, for funding through Vice Deanship of Scientific Research Chairs.

Conflicts of Interest: The authors declare no conflict of interest. The funders had no role in the design of the study; in the collection, analyses, or interpretation of data; in the writing of the manuscript, or in the decision to publish the results.

Sample Availability: Aliquots of samples are available from the authors.

References

1. Gudlaugsson, O.; Gillespie, S.; Lee, K.; Berg, J.V.; Hu, J.; Messer, S.; Herwaldt, L.; Pfaller, M.; Diekema, D. Attributable mortality of nosocomial candidemia, revisited. *Clin. Infect. Dis.* **2003**, *37*, 1172–1177. [[CrossRef](#)]
2. Antinori, S.; Milazzo, L.; Sollima, S.; Galli, M.; Corbellino, M. Candidemia and invasive candidiasis in adults: A narrative review. *Eur. J. Intern. Med.* **2016**, *34*, 21–28. [[CrossRef](#)]
3. Sudbery, P.E. Growth of *Candida albicans* hyphae. *Nat. Rev. Genet.* **2011**, *9*, 737–748. [[CrossRef](#)]
4. Gow, N.A.R.; Van De Veerdonk, F.L.; Brown, A.J.P.; Netea, M.G. *Candida albicans* morphogenesis and host defence: Discriminating invasion from colonization. *Nat. Rev. Genet.* **2011**, *10*, 112–122. [[CrossRef](#)] [[PubMed](#)]
5. Lu, Y.; Su, C.; Liu, H. *Candida albicans* hyphal initiation and elongation. *Trends Microbiol.* **2014**, *22*, 707–714. [[CrossRef](#)]
6. Gow, N.A.R.; Yadav, B. Microbe Profile: *Candida albicans*: A shape-changing, opportunistic pathogenic fungus of humans. *Microbiology* **2017**, *163*, 1145–1147. [[CrossRef](#)] [[PubMed](#)]

7. Sardi, J.C.O.; Scorzoni, L.; Bernardi, T.; Fusco-Almeida, A.M.; Giannini, M.J.S.M. Candida species: Current epidemiology, pathogenicity, biofilm formation, natural antifungal products and new therapeutic options. *J. Med. Microbiol.* **2013**, *62*, 10–24. [[CrossRef](#)]
8. Dantas, A.D.S.; Lee, K.K.; Raziunaite, I.; Schaefer, K.; Wagener, J.; Yadav, B.; Gow, N.A. Cell biology of *Candida albicans*–host interactions. *Curr. Opin. Microbiol.* **2016**, *34*, 111–118. [[CrossRef](#)]
9. Sanguinetti, M.; Posteraro, B.; Lass-Flörl, C. Antifungal drug resistance among *Candida* species: Mechanisms and clinical impact. *Mycoses* **2015**, *58*, 2–13. [[CrossRef](#)] [[PubMed](#)]
10. Cui, J.; Ren, B.; Tong, Y.; Dai, H.; Zhang, L. Synergistic combinations of antifungals and anti-virulence agents to fight against *Candida albicans*. *Virulence* **2015**, *6*, 362–371. [[CrossRef](#)] [[PubMed](#)]
11. Perfect, J.R. The antifungal pipeline: A reality check. *Nat. Rev. Drug Discov.* **2017**, *16*, 603–616. [[CrossRef](#)] [[PubMed](#)]
12. Qin, Y.; Zhang, L.; Xu, Z.; Zhang, J.; Jiang, Y.-Y.; Cao, Y.; Yan, T. Innate immune cell response upon *Candida albicans* infection. *Virulence* **2016**, *7*, 512–526. [[CrossRef](#)]
13. Silva, D.R.; Sardi, J.D.C.O.; Freires, I.A.; Silva, A.C.B.; Rosalen, P.L. In silico approaches for screening molecular targets in *Candida albicans*: A proteomic insight into drug discovery and development. *Eur. J. Pharm.* **2019**, *842*, 64–69. [[CrossRef](#)]
14. Howard, K.C.; Dennis, E.K.; Watt, D.S.; Garneau-Tsodikova, S. A comprehensive overview of the medicinal chemistry of antifungal drugs: Perspectives and promise. *Chem. Soc. Rev.* **2020**, *49*, 2426–2480. [[CrossRef](#)]
15. Whaley, S.G.; Berkow, E.L.; Rybak, J.M.; Nishimoto, A.T.; Barker, K.S.; Rogers, P.D. Azole antifungal resistance in *Candida albicans* and emerging non-*albicans* *Candida* species. *Front. Microbiol.* **2017**, *7*, 2173. [[CrossRef](#)] [[PubMed](#)]
16. Venugopala, K.N.; Chandrashekhara, S.; Alwassil, O.I.; Harsha, S.; Mlisana, K.; Odhav, B.; Pillay, M.; Bhandary, S.; Kandeel, M.; Mahomoodally, F.M.; et al. Synthesis and structural elucidation of novel benzothiazole derivatives as anti-tubercular agents: In-silico screening for possible target identification. *Med. Chem.* **2019**, *15*, 311–326. [[CrossRef](#)] [[PubMed](#)]
17. Siddesh, M.B.; Padmashali, B.; Thriveni, K.S.; Sandeep, C. Synthesis of thiophene-linked pyrimidopyrimidines as pharmaceutical leads. *J. Chem. Sci.* **2014**, *126*, 821–826. [[CrossRef](#)]
18. Thriveni, K.S.; Padmashali, B.; Siddesh, M.B.; Sandeep, C. Synthesis of pyrimidine incorporated piperazine derivatives and their antimicrobial activity. *Indian J. Pharm. Sci.* **2014**, *76*, 332–338.
19. Nagesh, K.B.; Padmashali, C.; Sandeep, T.C.M.; Yuvaraj, M.B.; Mallikarjuna, S.M. Synthesis and antimicrobial activity of benzothiophene substituted coumarins, pyrimidines and pyrazole as new scaffold. *Int. J. Pharm. Sci. Res.* **2014**, *28*, 6–10.
20. Nagesh, K.B.; Padmashali, C.; Sandeep, T.E.; Lokesh, M. Synthesis and characterization of novel benzothiophene substituted oxadiazole derivatives and their antimicrobial activity. *Der Pharm. Chem.* **2015**, *7*, 129–136.
21. Venugopala, K.N.; Chandrashekhara, S.; Bhandary, S.; Chopra, D.; Khedr, M.A.; Aldhubiab, B.E.; Attimarad, M.; Odhav, B. Efficient synthesis and characterization of novel substituted 3-benzoylindolizine analogues via the cyclization of aromatic cycloimmonium ylides with electron deficient alkenes. *Curr. Org. Synth.* **2018**, *15*, 388–395. [[CrossRef](#)]
22. Chandrashekhara, S.; Venugopala, K.N.; Nayak, S.K.; Gleiser, R.M.; Garcia, D.A.; Kumalo, H.M.; Kulkarni, R.S.; Mahomoodally, F.M.; Venugopala, R.; Mohan, M.K.; et al. One-pot microwave assisted synthesis and structural elucidation of novel ethyl 3-substituted-7-methylindolizine-1-carboxylates with larvicidal activity against *Anopheles arabiensis*. *J. Mol. Struct.* **2018**, *1156*, 377–384. [[CrossRef](#)]
23. Chandrashekhara, S.; Venugopala, K.N.; Tratat, C.; Mahomoodally, F.M.; Al-Dhubiab, B.E.; Haroun, M.; Venugopala, R.; Mohan, M.K.; Kulkarni, R.S.; Attimarad, M.V.; et al. Efficient synthesis and characterization of novel indolizines: Exploration of in vitro COX-2 inhibitory activity and molecular modelling studies. *New J. Chem.* **2018**, *42*, 4893–4901. [[CrossRef](#)]
24. Mallikarjuna, S.M.; Padmashali, M.S.M.B.; Chandrashekhara, S.; Sandeep, C. Synthesis, anticancer and antituberculosis studies for [1-(4-chlorophenyl) Cyclopropyl] (Piperazine-yl) Methanone derivatives. *Int. J. Pharm. Pharm. Sci.* **2014**, *6*, 423–427.
25. Mallikarjuna, S.M.; Chandrashekhara, S.P.B. Acid amine coupling of (1h-indole-6-yl) Piperazine-1-yl Methanone with substituted acids using hatu coupling reagent and their antimicrobial and antioxidant activity. *Int. J. Pharm. Sci. Res.* **2017**, *8*, 2879–2885. [[CrossRef](#)]
26. Sandeep, C.; Padmashali, B.; Kulkarni, R.S.; Mallikarjuna, S.M.; Siddesh, M.B.; Nagesh, H.K.; Thriveni, K.S. Synthesis of substituted 5-acetyl-3-benzoylindolizine-1-carboxylate from substituted 2-acetyl pyridinium bromides. *Heterocycl. Lett.* **2014**, *4*, 371–376.
27. Sandeep, C.; Venugopala, K.N.; Khedr, M.A.; Padmashali, B.; Kulkarni, R.S.; Venugopala, R.; Odhav, B. Design and synthesis of novel indolizine analogues as COX-2 inhibitors: Computational perspective and in vitro screening. *Indian J. Pharm. Educ. Res.* **2017**, *51*, 452–460. [[CrossRef](#)]
28. Sandeep, C.; Padmashali, B.; Venugopala, K.N.; Kulkarni, R.S.; Venugopala, R.; Odhav, B. Synthesis and characterization of ethyl 7-acetyl-2-substituted 3-(Substituted benzoyl) Indolizine-1-carboxylates for in vitro anticancer activity. *Asian J. Chem.* **2016**, *28*, 1043–1048. [[CrossRef](#)]
29. Sandeep, C.; Venugopala, K.N.; Gleiser, R.M.; Chetram, A.; Padmashali, B.; Kulkarni, R.S.; Venugopala, R.; Odhav, B. Greener synthesis of indolizine analogues using water as a base and solvent: Study for larvicidal activity against *Anopheles arabiensis*. *Chem. Biol. Drug Des.* **2016**, *88*, 899–904. [[CrossRef](#)]
30. Venugopala, K.N.; Al-Attraqchi, O.H.; Girish, M.B.; Chandrashekhara, S.; Alwassil, O.I.; Odhav, B.; Tratat, C.; Nayak, S.K.; Morsy, M.A.; Aldhubiab, B.E.; et al. Novel series of methyl 3-(Substituted benzoyl)-7-substituted-2-phenylindolizine-1-carboxylates as promising anti-inflammatory agents: Molecular modeling studies. *Biomolecules* **2019**, *9*, 661. [[CrossRef](#)] [[PubMed](#)]

31. Venugopala, K.N.; Tratratt, C.; Haroun, M.; Odhav, B.; Chandrashekarappa, S.; Attimarad, M.; Sreeharsha, N.; Nair, A.; Pottathil, S.; Venugopala, R.; et al. Anti-tubercular potency and computationally assessed drug-likeness and toxicology of diversely substituted indolizines. *Indian J. Pharm. Educ. Res.* **2019**, *53*, 545–552. [[CrossRef](#)]
32. Venugopala, K.N.; Chandrashekarappa, S.; Sreeharsha, N.; Morsy, M.A.; Pottathil, S.; Venugopala, R.; Odhav, B.; Mlisana, K.; Pillay, M.; Abdallah, H.H.; et al. Computational, crystallographic studies, cytotoxicity and anti-tubercular activity of substituted 7-methoxy-indolizine analogues. *PLoS ONE* **2019**, *14*, e0217270. [[CrossRef](#)] [[PubMed](#)]
33. Venugopala, K.N.; Tratratt, C.; Nair, A.B.; Sreeharsha, N.; Venugopala, R.; Chandrashekarappa, S.; Alwassil, O.I.; Odhav, B.; Pillay, M.; Mahomoodally, F.M.; et al. Anti-tubercular activity of substituted 7-methyl and 7-formylindolizines and in silico study for prospective molecular target identification. *Antibiotics* **2019**, *8*, 247. [[CrossRef](#)] [[PubMed](#)]
34. Venugopala, K.N.; Tratratt, C.; Pillay, M.; Chandrashekarappa, S.; Al-Attraqchi, O.H.A.E.; Aldhubiab, B.; Attimarad, M.I.; Alwassil, O.; Nair, A.B.; Sreeharsha, N.; et al. In silico design and synthesis of tetrahydropyrimidinones and tetrahydropyrimidinethiones as potential thymidylate kinase inhibitors exerting anti-TB activity against mycobacterium tuberculosis. *Drug Des. Dev. Ther.* **2020**, *ume 14*, 1027–1039. [[CrossRef](#)]
35. Venugopala, K.N.; Uppar, V.; Chandrashekarappa, S.; Abdallah, H.H.; Pillay, M.; Deb, P.K.; Morsy, M.A.; Aldhubiab, B.E.; Attimarad, M.; Nair, A.B.; et al. Cytotoxicity and Antimycobacterial Properties of Pyrrolo[1,2-a]quinoline Derivatives: Molecular Target Identification and Molecular Docking Studies. *Antibiotics* **2020**, *9*, 233. [[CrossRef](#)] [[PubMed](#)]
36. Hasija, A.; Bhandary, S.; Venugopala, K.N.; Chandrashekarappa, S.; Chopra, D. Structural investigation of methyl 3-(4-fluorobenzoyl)-7-methyl-2-phenylindolizine-1-carboxylate, an inhibitory drug towards Mycobacterium tuberculosis. *Acta Cryst. Sect. E Cryst. Commun.* **2020**, *76*, 567–571. [[CrossRef](#)] [[PubMed](#)]
37. Khedr, M.A.; Pillay, M.; Chandrashekarappa, S.; Chopra, D.; Aldhubiab, B.E.; Attimarad, M.; Alwassil, O.I.; Mlisana, K.; Odhav, B.; Venugopala, K.N. Molecular modeling studies and anti-TB activity of trisubstituted indolizine analogues; molecular docking and dynamic inputs. *J. Biomol. Struct. Dyn.* **2018**, *36*, 2163–2178. [[CrossRef](#)] [[PubMed](#)]
38. Sandeep, C.; Venugopala, K.N.; Khedr, M.A.; Attimarad, M.; Padmashali, B.; Kulkarni, R.S.; Venugopala, R.; Odhav, B. Review on chemistry of natural and synthetic indolizines with their chemical and pharmacological properties. *J. Basic Clin. Pharm.* **2017**, *8*, 49–60.
39. Chandrashekarappa, S.; Venugopala, K.N.; Venugopala, R.; Padmashali, B. Qualitative anti-tubercular activity of synthetic ethyl 7-acetyl-2-substituted-3-(4-substituted benzoyl) indolizine-1-carboxylate analogues. *J. Appl. Pharm. Sci.* **2019**, *9*, 124–128. [[CrossRef](#)]
40. Sandeep, C.; Padmashali, B.; Kulkarni, R.S. Efficient synthesis of indolizines and new imidazo[1,2-a]pyridines via the expected cyclization of aromatic cycloimmonium ylides with electron deficient alkynes and ethyl cyanofomate. *Tetrahedron Lett.* **2013**, *54*, 6411–6414. [[CrossRef](#)]
41. Sandeep, C.; Basavaraj, P.; Rashmi, S.K. Synthesis of isomeric substituted 6-acetyl-3-benzoylindolizine-1-carboxylate and 8-acetyl-3-benzoylindolizine-1-carboxylate from substituted 3-acetyl pyridinium bromides and their antimicrobial activity. *J. Appl. Chem.* **2013**, *2*, 1049–1052.
42. Østby, O.B.; Dalhus, B.; Gundersen, L.-L.; Rise, F.; Bast, A.; Haenen, G.R.M.M. Synthesis of 1-substituted 7-cyano-2,3-diphenylindolizines and evaluation of antioxidant properties. *Eur. J. Org. Chem.* **2000**, *2000*, 3763–3770. [[CrossRef](#)]
43. Baidya, M.; Kumar, J.; Srivastava, A.K.; Jyothi, C.; Gupta, A.; Das, A.K. Synthesis and pharmacological screening of some indolizine-amido glutamine amino acid derivatives. *Indian J. Heterocycl. Chem.* **2004**, *14*, 81–82.
44. Uppar, V.; Mudnakudu-Nagaraju, K.K.; Basarikatti, A.I.; Chougala, M.; Chandrashekarappa, S.; Mohan, M.K.; Banuprakash, G.; Venugopala, K.N.; Ningegowda, R.; Padmashali, B. Microwave induced synthesis, and pharmacological properties of novel 1-benzoyl-4-bromopyrrolo[1,2-a]quinoline-3-carboxylate analogues. *Chem. Data Collect.* **2020**, *25*, 100316. [[CrossRef](#)]
45. Das, A.K.; Mukherjee, I. Synthesis and antimicrobial activity of mannich bases of indolizine analogues. *Orient. J. Chem.* **2006**, *22*, 339–342.
46. Das, A.K.; Mukherjee, I. Synthesis and evaluation of some 3-benzoylindolizine-1-carboxamides as possible anti-inflammatory and analgesic agents. *Orient. J. Chem.* **2006**, *22*, 415–420.
47. Kallay, K.R.; Doerge, R.F. P-substituted 1,2-diphenylindolizines as anti-inflammatory agents. *J. Pharm. Sci.* **1972**, *61*, 949–951. [[CrossRef](#)] [[PubMed](#)]
48. James, D.A.; Koya, K.; Li, H.; Liang, G.; Xia, Z.; Ying, W.; Wu, Y.; Sun, L. Indole- and indolizine-glyoxylamides displaying cytotoxicity against multidrug resistant cancer cell lines. *Bioorg. Med. Chem. Lett.* **2008**, *18*, 1784–1787. [[CrossRef](#)] [[PubMed](#)]
49. Morita, K.; Yamamoto, I.H. Synthesis of indolizine derivatives. *Biochem. Pharmacol.* **1973**, *22*, 111–115.
50. Lingala, S.; Nerella, R.; Cherukupally, R.; Das, A.K. Synthesis and comparative anti-tubercular activity of indolizine derivatives of isoniazid/Pyrazinamide/Ethionamide. *Int. J. Pharm. Sci. Rev. Res.* **2011**, *6*, 128–131.
51. Liu, Y.; Zhang, Y.; Shen, Y.-M.; Hu, H.-W.; Xu, J.-H. Regioselective synthesis of 3-acylindolizines and benzo- analogues via 1,3-dipolar cycloadditions of N-ylides with maleic anhydride. *Org. Biomol. Chem.* **2010**, *8*, 2449–2456. [[CrossRef](#)]
52. Sharma, V.; Kumar, V. Indolizine: A biologically active moiety. *Med. Chem. Res.* **2014**, *23*, 3593–3606. [[CrossRef](#)]
53. Gómez, C.M.M.; Kouznetsov, V.V.; Sortino, M.A.; Álvarez, S.L.; Zacchino, S.A. In vitro antifungal activity of polyfunctionalized 2-(hetero)arylquinolines prepared through imino Diels–Alder reactions. *Bioorg. Med. Chem.* **2008**, *16*, 7908–7920. [[CrossRef](#)] [[PubMed](#)]

54. Vemula, V.R.; Vurukonda, S.; Bairi, C.K. Indolizine derivatives: Recent advances and potential pharmacological activities. *Int. J. Pharm. Sci. Rev. Res.* **2011**, *11*, 159–163.
55. Uppar, V.; Chandrashekarappa, S.; Basarikatti, A.I.; Banuprakash, G.; Mohan, M.; Chougala, M.; Mudnakudu-Nagaraju, K.K.; Ningegowda, R.; Padmashali, B. Synthesis, antibacterial, and antioxidant studies of 7-amino-3-(4-fluorobenzoyl)indolizine-1-carboxylate derivatives. *J. Appl. Pharm. Sci.* **2020**, *10*, 77–85. [[CrossRef](#)]
56. Uppar, V.; Chandrashekarappa, S.; Venugopala, K.N.; Deb, P.K.; Kar, S.; Alwassil, O.I.; Gleiser, R.M.; Garcia, D.; Odhav, B.; Mohan, M.K.; et al. Synthesis and characterization of pyrrolo[1,2-a]quinoline derivatives for their larvicidal activity against *Anopheles arabiensis*. *Struct. Chem.* **2020**, *31*, 1533–1543. [[CrossRef](#)]
57. Dillard, R.D.; Pavey, D.E.; Benslay, D.N. Synthesis and antiinflammatory activity of some 2,2-dimethyl-1,2-dihydroquinolines. *J. Med. Chem.* **1973**, *16*, 251–253. [[CrossRef](#)]
58. Sechi, M.; Rizzi, G.; Bacchi, A.; Carcelli, M.; Rogolino, D.; Pala, N.; Sanchez, T.W.; Taheri, L.; Dayam, R.; Neamati, N. Design and synthesis of novel dihydroquinoline-3-carboxylic acids as HIV-1 integrase inhibitors. *Bioorg. Med. Chem.* **2009**, *17*, 2925–2935. [[CrossRef](#)]
59. Dubé, D.; Blouin, M.; Brideau, C.; Chan, C.-C.; Desmarais, S.; Ethier, D.; Falguyret, J.-P.; Friesen, R.W.; Girard, M.; Girard, Y.; et al. Quinolines as potent 5-lipoxygenase inhibitors: Synthesis and biological profile of L-746,530. *Bioorg. Med. Chem. Lett.* **1998**, *8*, 1255–1260. [[CrossRef](#)]
60. Testa, M.L.; Lamartina, L.; Mingoia, F. A new entry to the substituted pyrrolo[3,2-c]quinoline derivatives of biological interest by intramolecular heteroannulation of internal imines. *Tetrahedron* **2004**, *60*, 5873–5880. [[CrossRef](#)]
61. Martins, C.; Carreiras, M.C.; Leon, R.; Rios, C.D.L.; Bartolini, M.; Andrisano, V.; Iriepa, I.; Moraleda, I.; Gálvez, E.; Garcia, M.; et al. Synthesis and biological assessment of diversely substituted furo[2,3-b]quinolin-4-amine and pyrrolo[2,3-b]quinolin-4-amine derivatives, as novel tacrine analogues. *Eur. J. Med. Chem.* **2011**, *46*, 6119–6130. [[CrossRef](#)] [[PubMed](#)]
62. Guha, R.; Bender, A. *Computational Approaches in Cheminformatics and Bioinformatics*; Wiley: Hoboken, NJ, USA, 2012.
63. Chakraborty, A.; Pan, S.; Chattaraj, P.K. Biological activity and toxicity: A conceptual dft approach. In *Structure and Bonding*; Springer International Publishing: Berlin/Heidelberg, Germany, 2013; pp. 143–179.
64. Pan, S.; Gupta, A.; Subramanian, V.; Chattaraj, P.K. Quantitative structure-activity/Property/Toxicity relationships through conceptual density functional theory-based reactivity descriptors. In *Sustainable Nanosystems Development, Properties, and Applications*; IGI Global: Hershey, PA, USA, 2015; pp. 123–179.
65. Pan, S.A.; Gupta, D.; Roy, R.; Sharma, V.; Subramanian, A.; Mitra, P.; Chattaraj, P. Application of conceptual density functional theory in developing qsar models and their usefulness in the prediction of biological activity and toxicity of molecules. In *Chemometrics Applications and Research*; Apple Academic Press: Palm Bay, FL, USA, 2016; pp. 183–214.
66. Kon’è, M.G.-R.; N’dri, J.S.; Kodjo, C.G.; Kablan, A.L.C.; Ouattara, L.; Ouattara, O. Combining of dft and qsar results to predict the antibacterial activity of a series of azetidiones derived from dapsone as inhibitors of bacillus subtilis and pseudomonas aeruginosa. *SDRP J. Comp. Chem. Mol. Model.* **2018**, *2*, 1–8.
67. Zermeño-Macías, M.D.L.Á.; González-Chávez, M.M.; Méndez, F.; González-Chávez, R.; Richaud, A. Theoretical reactivity study of indol-4-ones and their correlation with antifungal activity. *Molecules* **2017**, *22*, 427. [[CrossRef](#)] [[PubMed](#)]
68. Frau, J.; Muñoz, F.; Glossman-Mitnik, D. A molecular electron density theory study of the chemical reactivity of cis- and trans-resveratrol. *Molecules* **2016**, *21*, 1650. [[CrossRef](#)]
69. Flores-Holguín, N.; Frau, J.; Glossman-Mitnik, D. Computational peptidology assisted by conceptual density functional theory for the study of five new antifungal tripeptides. *ACS Omega* **2019**, *4*, 12555–12560. [[CrossRef](#)]
70. Rajpoot, M.; Bhattacharyya, R.; Sharma, A.K.; Gupta, G.K.; Kumar, V. 2. Drug designing in novel drug discovery: Trends, scope and relevance. In *Chemical Drug Design*; Springer: Berlin, Germany, 2016; pp. 15–30.
71. Gore, M.; Jagtap, U.B. *Computational Drug Discovery and Design*; Springer Science Business Media, LLC.: New York, NY, USA, 2018.
72. Parr, R.; Yang, W. *Density-Functional Theory of Atoms and Molecules*; Oxford University Press: New York, NY, USA, 1989.
73. Chermette, H. Chemical reactivity indexes in density functional theory. *J. Comput. Chem.* **1999**, *20*, 129–154. [[CrossRef](#)]
74. Geerlings, P.; De Proft, F.; Langenaeker, W. Conceptual density functional theory. *Chem. Rev.* **2003**, *103*, 1793–1873. [[CrossRef](#)]
75. Halgren, T.A. Merck molecular force field: I. Basis, form, scope, parameterization, and performance of mmff94. *J. Comput. Chem.* **1996**, *17*, 490–519. [[CrossRef](#)]
76. Halgren, T.A. Merck molecular force field. II. Mmff94 van der waals and electrostatic parameters for intermolecular inter-actions. *J. Comput. Chem.* **1996**, *17*, 520–552. [[CrossRef](#)]
77. Halgren, T.A. MMFF VI. MMFF94s Option for energy minimization studies. *J. Comput. Chem.* **1999**, *20*, 720–729. [[CrossRef](#)]
78. Halgren, T.A.; Nachbar, R.B. Merck molecular force field. IV. Conformational energies and geometries for MMFF94. *J. Comput. Chem.* **1996**, *17*, 587–615. [[CrossRef](#)]
79. Halgren, T.A. Merck molecular force field. V. Extension of MMFF94 using experimental data, additional computational data, and empirical rules. *J. Comput. Chem.* **1996**, *17*, 616–641. [[CrossRef](#)]
80. Frisch, M.J.; Trucks, G.W.; Schlegel, G.E.; Scuseria, M.A.; Robb, J.R.; Cheeseman, G.; Scalmani, V.; Barone, B.; Mennucci, G.A.; Petersson, H.; et al. *Gaussian 09 Revision E.01*; Gaussian Inc.: Wallingford, CT, USA, 2016.
81. Peverati, R.; Truhlar, D.G. Screened-exchange density functionals with broad accuracy for chemistry and solid-state physics. *Phys. Chem. Chem. Phys.* **2012**, *14*, 16187–16191. [[CrossRef](#)] [[PubMed](#)]

82. Weigend, F.; Ahlrichs, R. Balanced basis sets of split valence, triple zeta valence and quadruple zeta valence quality for H to Rn: Design and assessment of accuracy. *Phys. Chem. Chem. Phys.* **2005**, *7*, 3297–3305. [[CrossRef](#)] [[PubMed](#)]
83. Weigend, F. Accurate Coulomb-fitting basis sets for H to Rn. *Phys. Chem. Chem. Phys.* **2006**, *8*, 1057–1065. [[CrossRef](#)] [[PubMed](#)]
84. Flores-Holguín, N.; Frau, J.; Glossman-Mitnik, D. Conceptual dft as a helpful chemoinformatics tool for the study of the cla-vanin family of antimicrobial marine peptides. In *Density Functional Theory Calculations*; IntechOpen: Rijeka, Croatia, 2019; pp. 1–11.
85. Frau, J.; Glossman-Mitnik, D. Molecular reactivity and absorption properties of melanoidin blue-g1 through conceptual dft. *Molecules* **2018**, *23*, 559. [[CrossRef](#)]
86. Frau, J.; Glossman-Mitnik, D. Conceptual dft study of the local chemical reactivity of the dilysyldipyrrolones a and b in-intermediate melanoidins. *Chem. Acc.* **2018**, *137*, 1210. [[CrossRef](#)]
87. Frau, J.; Glossman-Mitnik, D. Conceptual dft study of the local chemical reactivity of the colored bisarg melanoidin and its protonated derivative. *Front. Chem.* **2018**, *6*, 136. [[CrossRef](#)]
88. Frau, J.; Glossman-Mitnik, D. Computational study of the chemical reactivity of the Blue-M1 intermediate melanoidin. *Comput. Chem.* **2018**, *1134*, 22–29. [[CrossRef](#)]
89. Frau, J.; Glossman-Mitnik, D. Chemical reactivity theory applied to the calculation of the local reactivity descriptors of a colored maillard reaction product. *Chem. Sci. Int. J.* **2018**, *22*, 1–14. [[CrossRef](#)]
90. Frau, J.; Glossman-Mitnik, D. Blue M2: An intermediate melanoidin studied via conceptual DFT. *J. Mol. Model.* **2018**, *24*, 138. [[CrossRef](#)]
91. Marenich, A.V.; Cramer, C.J.; Truhlar, D.G. Universal solvation model based on solute electron density and on a continuum model of the solvent defined by the bulk dielectric constant and atomic surface tensions. *J. Phys. Chem. B* **2009**, *113*, 6378–6396. [[CrossRef](#)] [[PubMed](#)]
92. Flores-Holguín, N.; Frau, J.; Glossman-Mitnik, D. A fast and simple evaluation of the chemical reactivity properties of the Pristinamycin family of antimicrobial peptides. *Chem. Phys. Lett.* **2020**, *739*, 137021. [[CrossRef](#)]
93. Flores-Holguín, N.; Frau, J.; Glossman-Mitnik, D. Conceptual dft-based computational peptidology of marine natural compounds: Dis- codermis a–h. *Molecules* **2020**, *25*, 4158. [[CrossRef](#)]
94. Flores-Holguín, N.; Frau, J.; Glossman-Mitnik, D. Virtual screening of marine natural compounds by means of chemoinformatics and cdft-based computational peptidology. *Mar. Drugs* **2020**, *18*, 478. [[CrossRef](#)] [[PubMed](#)]
95. Frau, J.; Glossman-Mitnik, D. Molecular reactivity of some maillard reaction products studied through conceptual DFT. *Contemp. Chem.* **2018**, *1*, 1–14.
96. Gázquez, J.; Cedillo, A.; Vela, A. Electrodonating and electroaccepting powers. *J. Phys. Chem.* **2007**, *111*, 1966–1970.
97. Chattaraj, P.K.; Chakraborty, A.; Giri, S. Net electrophilicity. *J. Phys. Chem. A* **2009**, *113*, 10068–10074. [[CrossRef](#)]
98. Jaramillo, P.; Domingo, L.R.; Chamorro, E.; Pérez, P. A further exploration of a nucleophilicity index based on the gas-phase ionization potentials. *J. Mol. Struct.* **2008**, *865*, 68–72. [[CrossRef](#)]
99. Daina, A.; Michielin, O.; Zoete, V. SwissTargetPrediction: Updated data and new features for efficient prediction of protein targets of small molecules. *Nucleic Acids Res.* **2019**, *47*, W357–W364. [[CrossRef](#)]
100. Daina, A.; Michielin, O.; Zoete, V. SwissADME: A free web tool to evaluate pharmacokinetics, drug-likeness and medicinal chemistry friendliness of small molecules. *Sci. Rep.* **2017**, *7*, 42717. [[CrossRef](#)] [[PubMed](#)]
101. Prasad, A.; Govindaraju, S.; Sushma, P.; Jain, A.S.; Chandan, D.; Prasad, M.N.N.; Kollur, S.P.; Srinivasa, C.; Shivamallu, C. Helicobacter pylori infection: A bioinformatic approach. *Int. J. Pharm. Sci. Res.* **2020**, *11*, 5469–5483.
102. O’Boyle, N.M.; Banck, M.A.; James, C.; Morley, C.; Vandermeersch, T.; Hutchison, G.R. Open Babel: An open chemical toolbox. *J. Cheminform.* **2011**, *3*, 33. [[CrossRef](#)]
103. Jain, A.S.; Sushma, P.; Chandan, D.; Beelagi, M.S.; Shashank, P.; Chandan, S.; Prasad, A.; Syed, A.; Marraiki, N.; Prasad, K.S. Effect of flavonoids having anti-inflammatory and antiviral properties on the spike glycoprotein of SARS-CoV-2: An In silico Approach. *Saudi J. Biol. Sci.* **2020**, *28*, 1040–1051. [[CrossRef](#)]
104. Prasad, S.K.; Sushma, P.; Chandan, S.; Kollur, S.P.; Syed, A.; Castro, J.O.; Frau, J.; Holguín, N.F.; Mitnik, D.G. Evaluating annona muricata acetogenins as possible anti-sars-cov-2 agents through in silico analysis and theoretical chemistry approaches. *Front. Chem.* **2021**, *8*, 624716. [[CrossRef](#)] [[PubMed](#)]
105. Dallakyan, S.; Olson, A.J. Small-molecule library screening by docking with PyRx. In *NMR-Based Metabolomics*; Springer Science and Business Media, LLC.: Berlin/Heidelberg, Germany, 2015; Volume 1263, pp. 243–250.